AGU PUBLICATIONS

JGR

Journal of Geophysical Research: Space Physics

RESEARCH ARTICLE
10.1002/2015JA021668

Key Points:
- Pi2 pulsations are associated with BBFs at various radial distances in the plasma sheet
- The Pi2 pulsations ahead of BBFs are usually in several discrete wave bands
- The majority of Pi2 waves ahead of BBFs are in slow-mode magnetosonic waves

Correspondence to:
X. Xing,
xyxingchen@gmail.com

Citation:
Xing, X., C.-P. Wang, J. Liang, and L. R. Lyons (2015), Plasma sheet Pi2 pulsations associated with bursty bulk flows, *J. Geophys. Res. Space Physics*, *120*, 8692–8706, doi:10.1002/2015JA021668.

Received 10 JUL 2015
Accepted 21 SEP 2015
Accepted article online 28 SEP 2015
Published online 27 OCT 2015

Plasma sheet Pi2 pulsations associated with bursty bulk flows

Xiaoyan Xing[1], Chih-Ping Wang[1], Jun Liang[2], and Larry R. Lyons[1]

[1]Department of Atmospheric and Oceanic Science, University of California, Los Angeles, California, USA, [2]Department of Physics and Astronomy, University of Calgary, Calgary, Alberta, Canada

Abstract There is a debate as to whether magnetic Pi2 pulsations (0.006–0.025 Hz) observed in the plasma sheet and on the ground are triggered by the earthward moving bursty bulk flows (BBFs) from midtail or distant tail or are caused by the substorm plasma instabilities initiated in the near-Earth plasma sheet. To resolve this debate, we conducted case and statistical studies of enhanced plasma sheet Pi2 pulsations using Time History of Events and Macroscale Interactions during Substorms (THEMIS) observations from $X\sim-30\,R_E$ to $X\sim-8\,R_E$. The case studies show that for both substorm-related and quiet time BBFs, enhanced Pi2 oscillations are observed in front of BBFs from midtail to the near-Earth plasma sheet. The oscillations intensify 1–4 min prior to the substantial flow enhancement, and usually initiate within several narrow discrete frequency bands, with lower frequencies intensifying earlier. We further examined the wave properties using low-frequency MHD fitting method and found that one or more discrete waves for each event are magnetosonic waves. Our statistical study of 364 BBFs shows that Pi2 pulsations are commonly associated with BBFs throughout the plasma sheet. The lowest-frequency oscillations usually appear below 0.01 Hz, and the strongest power oscillations appear at ~0.01 Hz or higher frequencies. We found that over 75% of the discrete oscillations are magnetosonic waves, and that 70%–75% of them are slow mode. These suggest that plasma sheet Pi2 pulsations are likely triggered by BBFs in the entire plasma sheet regardless of substorm onsets.

1. Introduction

Low-frequency magnetic oscillations within the Pi2 range observed on the ground have been generally accepted as a common feature associated with substorm onset [*Saito et al.*, 1976; *Yoeman et al.*, 1994; *Holter et al.*, 1995]. Plasma sheet in situ observations captured Pi2 pulsations (0.006–0.025 Hz) emerging 1–3 min prior to the substorm expansion onset in the near-Earth plasma sheet [*Lui and Najmi*, 1997; *Sigsbee et al.*, 2002; *Shiokawa et al.*, 2005; *Saito et al.*, 2008; *Liang et al.*, 2009; *Park et al.*, 2010], which is consistent with the ground signatures. Ground optical observations showed that oscillations within the Pi2 range can be observed along the growth phase arc before the auroral expansion occurs [*Uritsky et al.*, 2009; *Nishimura et al.*, 2014], and conjugate spacecraft have observed low-frequency magnetic oscillations correspondingly [*Uritsky et al.*, 2009], indicating the optical oscillations are a manifestation of the plasma sheet waves. The consistent sequence in both the plasma sheet and ionosphere suggest that the Pi2 pulsations prior to substorm onset are important transitional stage for the plasma sheet to develop from undisturbed to highly disturbed status. Thus, identifying the trigger of Pi2 pulsations in the plasma sheet may help reveal the key process for substorm onset initiation.

Observations have shown that the midlatitude ground Pi2 pulsations are closely related to the bursty bulk flows (BBFs) [e.g., *Angelopoulos et al.*, 1992] observed in the plasma sheet with oscillatory variations in the speed [*Kepko and Kivelson*, 1999]. The compressional pulse and the braking of flows may lead to these ground pulsations [*Kepko et al.*, 2001]. A similar relation was found for nonsubstorm period. *Sutcliffe and Lyons* [2002] and *Kim et al.* [2005] have found that high-latitude ground Pi2 pulsations during very quiet conditions can be observed in good correlation with auroral poleward boundary intensifications (PBIs), which are suggested to be associated with BBFs. From MHD wave analysis, *Wolf et al.* [2012] suggested that the oscillatory braking of the flows may cause the pulsations in Pi2 range, and this was supported by observations of *Panov et al.* [2013, 2014] in the plasma sheet. *Wang et al.* [2015] conducted a statistical study of large-amplitude Pi2 waves in the plasma sheet and found that nearly 80% of their events are associated with BBFs. Given the observations by *Runov et al.* [2014] that compressional oscillations can propagate farther earthward after the fast flow stops, the correlation between Pi2 waves and BBFs could be higher due to the spacecraft orbit's limitation in

capturing BBFs. This correlation has also been validated by auroral observations. Auroral streamers, which are ionospheric manifestation of plasma sheet BBFs, show one-to-one correlation with the ground Pi2 pulsations [*Nishimura et al*., 2012], indicating plausible triggering of the pulsations by BBFs.

On the other hand, theoretical studies have suggested that plasma sheet Pi2 pulsations can be a manifestation of ballooning mode instability, which is one of the candidate instabilities for leading to substorm onset and is likely initiated in the transition region between dipolar and tail-like field [*Erickson et al*., 2000; *Cheng and Zaharia*, 2004]. Many observations of magnetic oscillations within the Pi2 range near the transition region have used the ballooning instability theory for interpreting their observed pulsations [e.g., *Saito et al*., 2008; *Park et al*., 2010; *Panov et al*., 2012] but without other direct evidence for instability occurrence. This connection was directly validated by observations of *Xing et al*. [2013] through one case study, where Pi2 pulsations were found to intensify exactly when the MHD ballooning unstable criterion was satisfied prior to a small substorm. However, *Xing et al*. [2013] also observed an earthward flow burst slightly tailward of the unstable region prior to the instability initiation, which may have stopped before reaching the transition region, indicating that the BBF may have played some role in leading to the Pi2 pulsations and the instability. These observations have brought forward the question of whether plasma sheet Pi2 pulsations associated with substorm onset in fact result from earthward penetrating BBFs from the midtail or distant tail, which are commonly associated with substorms, or result from instabilities initiated in the transition region.

To resolve this problem, it is necessary to examine whether the Pi2 pulsations are, in general, correlated with BBFs or with ballooning instabilities in the plasma sheet. It is difficult to find direct evidence for instability initiation in the plasma sheet. However, BBFs signatures are straightforward to identify. Thus, in this study, we examine the magnetic oscillations associated with BBFs in the plasma sheet and identify whether pulsations within the Pi2 range are common features. For comparison to those Pi2 pulsations found in the transition region, BBFs at all radial distances from the midtail to the near-Earth region are employed, and the characteristics of the waves are examined. We use observations from five Time History of Events and Macroscale Interactions during Substorms (THEMIS) [*Angelopoulos*, 2008] probes with orbits covering from $X{\sim}-30\,R_E$ to $X{\sim}-8\,R_E$ during the 2008–2009 tail seasons. Magnetic field data are obtained from the Fluxgate Magnetometer [*Auster et al*., 2008]; particles data are obtained from both electrostatic analyzer [*McFadden et al*., 2008] and solid state telescope particle detectors, which cover the particle energy range from 5 eV to 6 MeV for ions and 5 eV to 1 MeV for electrons.

In section 2, three case studies are presented for details of BBFs and Pi2 pulsations at several different radial distances between -30 R_E and -8 R_E, with one quiet time event and two substorm-related events. Multispacecraft observations of the same BBF are shown. Section 3 shows statistical results of the correlations between Pi2 pulsations and BBFs and wave properties for 364 BBFs. The conclusions are summarized in section 4.

2. Pi2 Pulsations Associated With BBFs in the Plasma Sheet

First, we introduce the selection criteria for BBFs used in this study. We have selected events having substantial flow enhancement with peak value larger than 150 km/s and associated with dipolarization, which is defined as abrupt B_z enhancement of at least 5 nT within less than 10 s, and plasma $\beta > 0.5$ (ratio between plasma and magnetic pressures).

2.1. Pi2 Pulsations Associated With BBF in Midtail Plasma Sheet During Quite Time

In order to examine the correlations between Pi2 pulsations and BBFs during nonsubstorm periods, we have selected an isolated BBF event observed in the midtail plasma sheet on 3 February 2009. "Isolated" is defined as single flow peak associated with dipolarization without other abrupt disturbances within a 1 h time window. The *AE* index was lower than 50 for nearly 20 h before the selected time interval of BBF and over 10 h afterward. The aurora images in Figure 1 show a localized brightening (identified by the blue arrows) observed by THEMIS ground imager at Rankin Inlet (RANK) at around 72° magnetic latitude near 0.5 magnetic local time (MLT) at ~07:26 UT without further expansion, which indicates a poleward boundary intensification (PBI) [*Zesta et al*., 2002]. The THEMIS probe THB has its footprint mapped to the vicinity of the PBI, as shown by the red squares in Figure 1, and observed the signatures of a BBF.

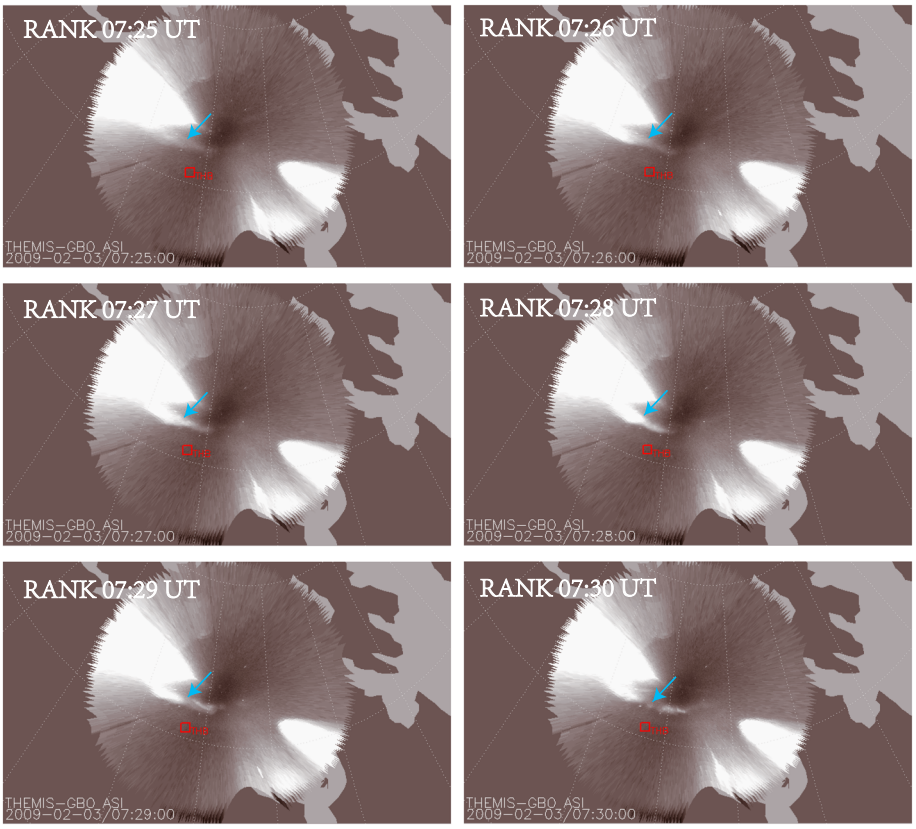

Figure 1. Auroral all-sky image from station of Rankin Inlet at six times on 3 February 2009.

Figure 2 shows the observations of magnetic field, bulk flow velocity in geocentric solar magnetospheric (GSM) coordinates, magnetic, thermal and total pressures, and plasma β and magnetic wavelet power spectrogram (in log(nT^2)) in two perpendicular and parallel directions ($\delta B_{\perp y}$ points toward dusk, and $\delta B_{\perp x}$ completes the right-hand system), respectively, from THB located at $X\sim-30\,R_E$. In the spectrogram analyses, continuous wavelet transform has been employed [*Torrence and Compo*, 1998]. This multiresolution technique uses varied spectra window for every single spectra component, thus well balances the trade-off of time-frequency resolution, which allows us to obtain desired resolution of both time and frequency in spectral features of a fluctuated data set. The scale factor, which is defined as 1/frequency and indicates the frequency resolution, is set to 2δt in our study (δt is the time spacing of the data series). The sampling rate within frequency range of [0.005, 0.02] Hz is 610, which gives us an extremely smooth picture of wavelet power.

The magnetic field shown in Figure 2 was steady prior to 07:27 UT, and a dipolarization is observed at ~07:27:15 UT (We identify this time to be at the most sharp increase of B_z). A moderate earthward bulk flow enhancement is found to be associated with the dipolarization. The spacecraft was located near the central plasma sheet during the entire time interval. The magnetic spectrograms show enhanced oscillations initiated at ~07:24 UT, nearly 3 min before the dipolarization. The oscillations initiate at several discrete frequency ranges between 0.006 and 0.025 Hz during the first 2–3 min with lower frequency appearing earlier and become more continuous and extend to higher frequencies after the dipolarization. It is necessary to point out that manual identification of timing of the enhanced oscillations is not accurate. There could be several to over 10 s time error due to vision difference. However, it is more important to identify the association between the enhanced oscillations with the dipolarizations than accurately determine the relative timing between them. Furthermore, 10 s time error does not essentially change the relative timing between the oscillations and dipolarizations, which are usually apart in the order of minutes. Thus, visual identification is adequate enough for our purpose. The results shown above are consistent with the observations of low-frequency magnetic oscillations initiation in the near-Earth region at $X\sim-11\,R_E$ by *Park et al.* [2010] and support the theoretical analysis of *Seboldt* [1990] and *Lee and Hau* [2008] that oscillations within the

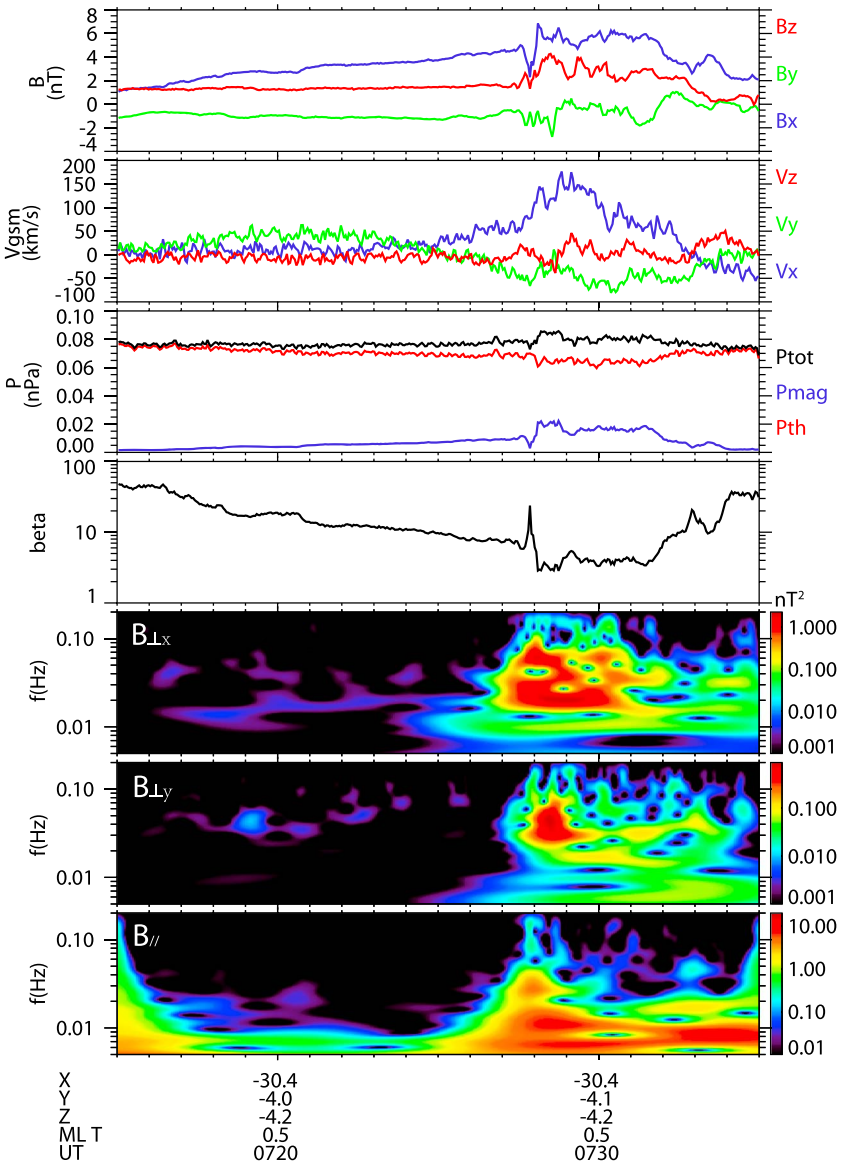

Figure 2. THB observations of (first panel) magnetic field in GSM, (second panel) bulk flow velocities in GSM, (third panel) thermal, magnetic, and total pressures, (fourth panel) plasma β, (fifth to seventh panels) magnetic field spectrograms in perpendicular directions *x* (earthward) and *y* (duskward) and parallel direction, respectively, on 3 February 2009.

MHD regime triggered in a Harris-type field configuration are likely to be in discrete frequencies. This case is found during very quiet time, indicating that plasma sheet Pi2 pulsations are not necessarily associated with a substorm onset but can be directly driven by BBFs and provide a possible source mechanism for high-latitude ground Pi2 pulsations as observed by *Sutcliffe and Lyons* [2002].

To further examine the wave properties, we employed the low-frequency wave fitting method developed by *Saito et al.* [2008] and analyzed the wave types of the enhanced oscillations. This method fits the observed magnetic field and bulk flow velocity using MHD momentum and induction equations. It defines the correlations between ($\delta B_{\parallel}$, $k_{\perp}\delta v_{\perp}/\omega$), ($\delta B_{\perp x}$, $\delta v_{\perp x}$), and ($\delta B_{\perp y}$, $\delta v_{\perp y}$) through relations of $\frac{\delta B_{\parallel}}{B_0} = \frac{k_{\perp}\delta v_{\perp}}{\omega}$ and $\frac{\delta B_{\perp j}}{B_0} = -\frac{k_{\parallel}\delta v_{\perp j}}{\omega}$, where *j* represents either *x* or *y* direction. Good correlations of the first two pairs of data sets represent magnetosonic waves, and that of the third pair represents Alfvenic wave. The magnetosonic wave phase velocity $\frac{\omega}{k_{\perp}}$ can be obtained from the least squares fitting of observed data set $\frac{\delta B_{\parallel}}{B_0}$ and $\delta v_{\perp}$. *Saito et al.* [2008] applied the fitting analysis over the entire frequency band of 0.006–0.025 Hz (named f_0 in our work). They identified

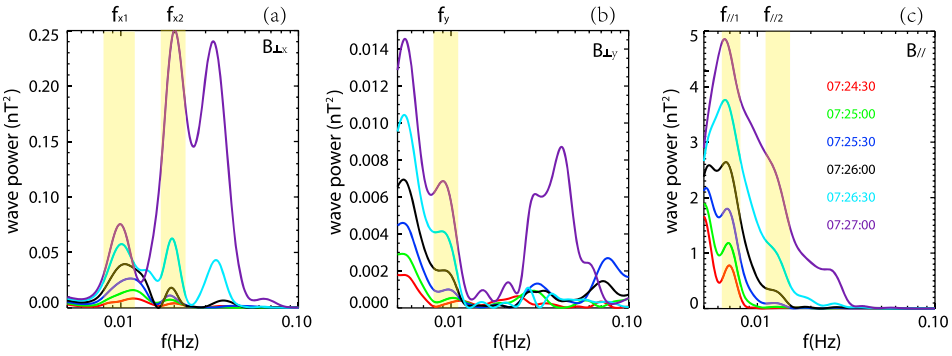

Figure 3. Line plots of magnetic field spectrograms at six selected times (identified in different colors) before dipolarization for perpendicular directions (a) *x*, (b) *y*, and (c) parallel direction.

slow-mode and fast-mode compressional waves ~3 min and ~1.5 min, respectively, prior to a magnetic dipolarization. However, the coexisting of the oscillations at different discrete frequency bands within the entire Pi2 range may mix different type of waves together and wipe out the properties of each discrete wave in MHD analysis. Thus, we apply the fitting method to each frequency band to obtain specific properties for each discrete wave. Figures 3a–3c show line plots of oscillation wave powers sliced at six different times from the three magnetic component $\delta B_{\perp x}$, $\delta B_{\perp y}$, and $\delta B_{//}$. The yellow shaded strips identify the enhanced discrete oscillation bands within 0.006–0.025 Hz. For each component, there are one or two discrete frequency bands identified within the f_0 range with $f_{x1} = 0.008$–0.012 Hz; $f_{x2} = 0.017$–0.023 Hz; $f_y = 0.008$–0.011 Hz; $f_{//1} = 0.006$–0.008 Hz, and $f_{//2} = 0.0105$–0.015 Hz ($f_{//2}$ can be identified at 07:25:30 UT and 07:26:00 UT but quickly became overwhelmed by the wave expansion in $f_{//1}$ band).

The results for MHD low-frequency analysis are shown in Figure 4. The first column shows the correlation between ($\delta B_{\parallel}/B_0$, $k_{\perp}\delta v_{\perp}/\omega$) with $k_{\perp}/\omega$ obtained from the least squares fitting method [*Saito et al.*, 2008]. Figure 4 (middle and right columns) show the scatterplots of ($\delta B_{\perp x}/B_0$, $\delta v_{\perp x}$) and ($\delta B_{\perp y}/B_0$, $\delta v_{\perp y}$), respectively. The oscillations in Figure 4 (top row) are calculated within the f_0 range, which is the entire frequency domain examined in our study. Figure 4 (middle and bottom rows) is obtained within each frequency band as labeled above the plot. The correlation coefficients, which are defined as the measure of linear correlation between two sets of variables, are given at the upper left corner in each plot. To include at least one full wave period in each calculation, we only examined the oscillations that intensify at least $1/f_{\min}$ prior to the dipolarization, where $f_{\min}$ is the minimum value of each frequency band. Thus, the correlation of ($\delta B_{\perp y}/B_0$, $\delta v_{\perp y}$) for f_y range is omitted because the $\delta B_{\perp y}$ oscillation within this frequency range intensified at ~07:26:00 UT, which is only ~70 s prior to the dipolarization; however, $1/f_y$ is within 91–125 s. Figure 4 (top row) shows that the correlation of each pair of variables is not strong, indicating that neither magnetosonic nor Alfvenic waves are found for frequency range f_0. However, as the fitted frequency confined to each discrete band, ($\delta B_{\parallel}/B_0$, $k_{\perp}\delta v_{\perp}/\omega$) within $f_{//1}$ and $f_{//2}$ bands and ($\delta B_{\perp x}/B_0$, $\delta v_{\perp x}$) within f_{x1} band show perfect correlations with coefficients around 0.99. This suggests that for the parallel component within both discrete frequency bands $f_{//1}$ and $f_{//2}$, the parallel magnetic fluctuations fit to the equation of magnetosonic waves. For $\delta B_{\perp x}$ which is perpendicular oscillations in the roughly earthward component, the wave within f_{x1} band fits perfectly to magnetosonic mode as well. The second frequency band f_{x2} in this component does not show good correlation, indicating some other type of waves that cannot be explained by the MHD equations. These fitting results show evidence that magnetosonic waves were present ahead of the dipolarization associated with the earthward moving flow at X~$-30\,R_E$, which is similar to those seen before substorm-related dipolarizations observed near the transition region [*Saito et al.*, 2008].

To further identify the mode of the three magnetosonic waves found above, we examined the phase relation of thermal and magnetic pressures for each frequency band. Figure 5 shows the waveforms of thermal pressure (dP_i in red) and magnetic pressure (dP_b in blue) filtered in the $f_{//1}$, $f_{//2}$, and f_{x1} frequency bands in the first three panels, and Alfvenic speed (V_a) in red and sound speed (V_s) in black in the fourth panel. The three black rectangles identify the time interval during which the data were used in the fitting analysis. dP_i and dP_b are nearly antiphase within the $f_{//1}$ range, and the fitted wave phase velocity is ~96 km/s, which is much lower

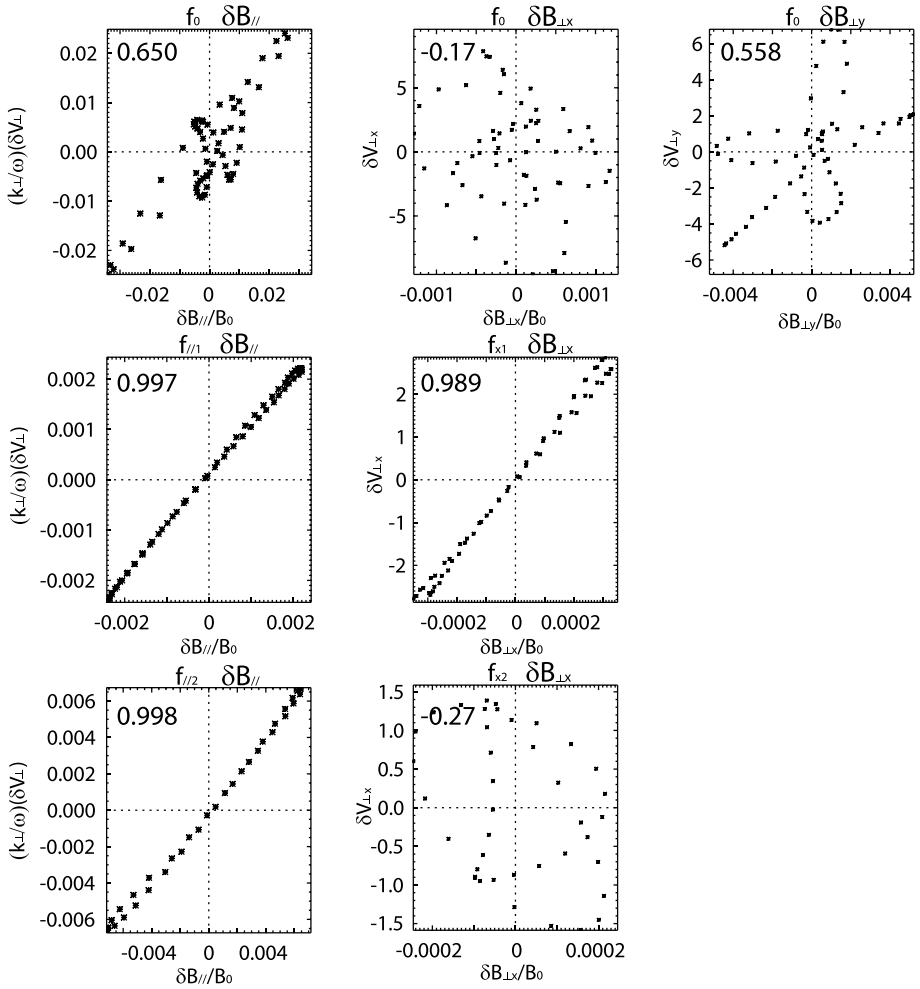

Figure 4. Low-frequency fitting results obtained from THB. (left column) Correlation between $(\delta B_{\parallel}/B_0, (k_{\perp}/\omega)\delta V_{\perp})$ for frequencies (top row) f_0, (middle row) $f_{//1}$, and (bottom row) $f_{//2}$. (middle column) Scatterplots of $\delta B_{\perp x}/B_0$ versus $\delta V_{\perp x}$ for frequencies f_0 in Figure 4 (top row), f_{x1} in Figure 4 (middle row), and f_{x2} in Figure 4 (bottom row). (right column) Scatterplots of $\delta B_{\perp y}/B_0$ versus $\delta V_{\perp y}$ for f_0.

than both Alfvenic and acoustic velocities, suggesting a slow-mode magnetosonic wave. dP_i and dP_b within $f_{//2}$ and f_{x1} range are neither in phase nor antiphase. The fitted wave phase velocities are 345 km/s, larger than V_a and bounded by V_s, and 198.85 km/s, lower than V_s and slightly lower than V_a. We suspect that both fast mode and slow mode exist for these two waves, so that the velocity reaches or approaches the fast mode but the phase relation between dP_i and dP_b is mixed by the two modes.

2.2. Pi2 Pulsation Associated With an Earthward Moving BBF at Two Radial Distances

After identifying that a BBF associated Pi2 pulsation event in midtail has the same properties as the substorm-related waves observed in the near-Earth region, we examine whether these enhanced waves appear ahead of more BBF events and how the waves evolve as BBFs move toward the Earth. We selected a BBF event observed by multispacecraft (THB and THC) aligned radially on 27 February 2009. *Runov et al.* [2009] analyzed this event as an expansion phase earthward propagating BBF. *Lyons et al.*, [2012] examined the detailed auroral images associated with this event and verified that the observed flows at these two different spacecraft locations are associated with one auroral streamer caused by the same earthward moving BBF. Thus, the Pi2 waves observed at these two spacecraft locations reveal the wave change as the plasma penetrates earthward.

Figure 6 shows the magnetic field, bulk flow velocity, and three components of magnetic spectrograms observed by THB at $X\sim-20.1\,R_E$ on the left and THC at $X\sim-16.7\,R_E$ on the right. Both spacecraft observed strong flows associated with dipolarizations. The vertical magenta lines identify the dipolarization time

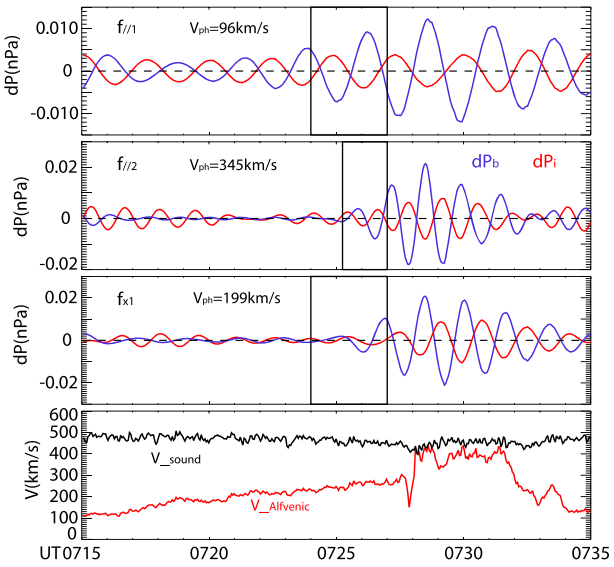

Figure 5. Pressure waveforms filtered at frequencies (first panel) $f_{//1}$, (second panel) $f_{//2}$, and (third panel) f_{x1} in the first three panels. (fourth panel) Alfvenic speed in red and sound speed in black.

at each spacecraft location. The dipolarization front propagated from $X\sim-20.1\,R_E$ to $X\sim-16.7\,R_E$ in about 60 s, indicating propagation speed of ~350 km/s. The magnetic spectrogram shows pronounced background oscillations due to the fact that the plasma sheet is highly disturbed during the substorm expansion phase. The auroral images show that the plasma sheet is very active for this event. The expansion onset that preceded this BBF occurred at ~07:45 UT, and expansions at other MLTs can be found at even earlier times. The magnetic oscillations associated with the BBF are substantially larger than the background oscillations for all the components at both spacecraft locations. Each component shows that the oscillation enhancements started with discrete frequency bands and then expanded in frequency range as time evolves.

Figure 7 shows line plots of the oscillation wave power obtained from THB (a–c) and THC (d–f) for $\delta B_{\perp x}$ (a and d), $\delta B_{\perp y}$ (b and e), and $\delta B_{\parallel}$ (c and f). The yellow shaded strips identify the oscillations that enhance with time within the Pi2 band with the name of each frequency band shown above the plot. The frequency range of all the bands is listed in Table 1.

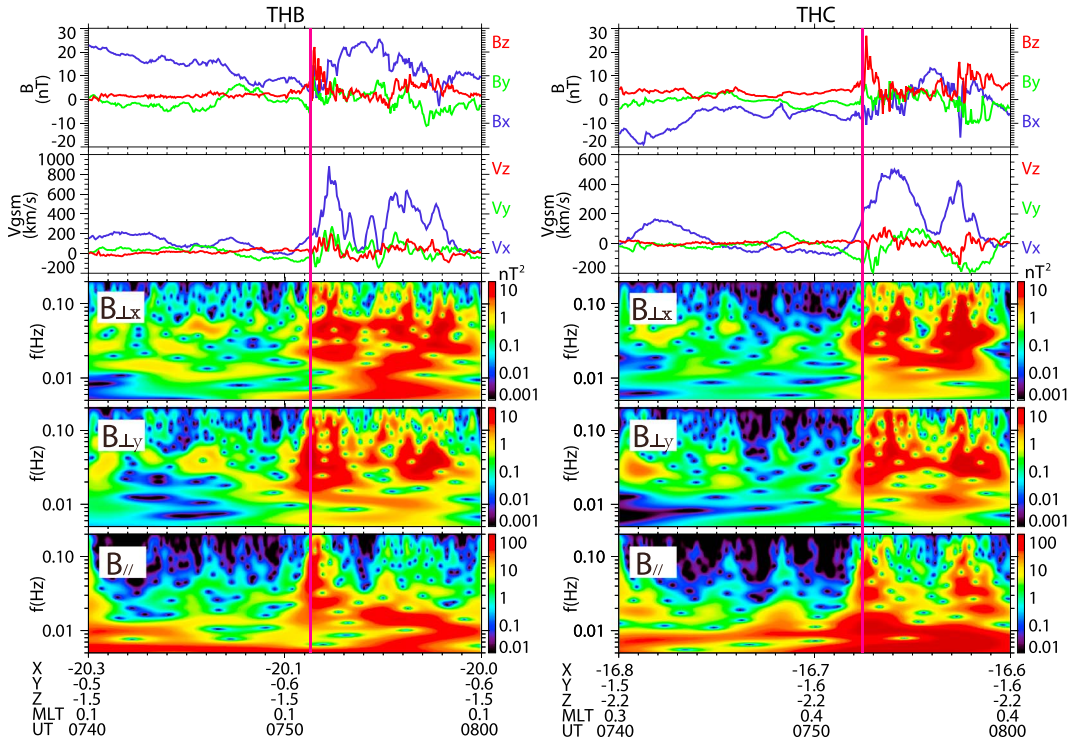

Figure 6. Magnetic field, bulk flow velocity, and three component of magnetic field spectrograms observed by (left) THB and (right) THC on 27 February 2009.

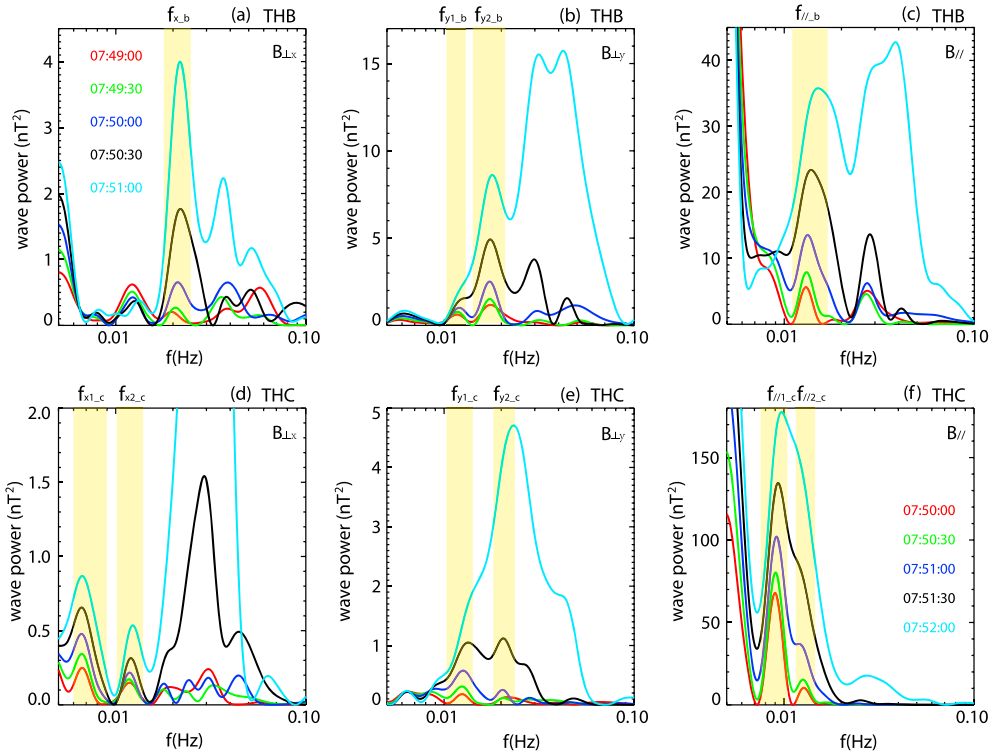

Figure 7. Line plots of magnetic field spectrograms observed by (a–c) THB and (d–f) THC. Three columns represent two perpendicular directions and parallel direction. The lines are sliced at five different times in different colors.

The wave analysis in the entire Pi2 band show weak correlation for each oscillation component (not shown here), similar to those found for 3 February 2009 event. Here we show the fitting results of every frequency band in Figure 8 with THB data in the first row and THC data in the second and third rows. The correlation between ($\delta B_{\parallel}/B_0$, $k_{\perp}\delta v_{\perp}/\omega$) in Figure 8 (first column) for the frequency bands $f_{//\_b}$ and $f_{//1\_c}$ is nearly 1, indicating perfect magnetosonic waves observed ahead of the BBF both at THB and THC locations. The correlation for $f_{//2\_c}$ is low, suggesting that the enhanced oscillation within 0.0115–0.0145 Hz cannot be interpreted by the low-frequency wave fitting analysis within the MHD regime. The correlations of the perpendicular magnetic disturbances with perpendicular flows are moderate or weak except for ($\delta B_{\perp y}/B_0$, $\delta v_{\perp y}$) within f_{y2_b} frequency band and ($\delta B_{\perp x}/B_0$, $\delta v_{\perp x}$) within f_{x2_c} frequency band. The correlation coefficient of −0.9 between $\delta B_{\perp y}/B_0$ and $\delta v_{\perp y}$ in f_{y2_b} band suggests that Alfven wave can be observed at the THB location while the magnetosonic wave is present. The correlation coefficient of −0.86 between $\delta B_{\perp y}/B_0$ and $\delta v_{\perp y}$ may indicate a magnetosonic wave effect on the oscillations in f_{x2_c} frequency band. However, other waves that cannot be explained by this fitting method should exist within this frequency band at the same time, lowering the correlation coefficient.

In Figure 9, we show the waveforms of the plasma and magnetic pressures for the two perfect magnetosonic waves ($f_{//\_b}$ of THB and $f_{//1\_c}$ of THC) and the two characteristic speeds (Alfvenic and sound) obtained from

Table 1. List of Frequency Bands and Their Frequency Ranges Analyzed for the 27 February 2009 Event

THB		THC	
Frequency Label	Frequency Range	Frequency Label	Frequency Range
f_{x_b}(Hz)	0.018–0.025	f_{x1_c}(Hz)	0.006–0.008
f_{y1_b}(Hz)	0.0102–0.013	f_{x2_c}(Hz)	0.01–0.014
f_{y2_b}(Hz)	0.014–0.021	f_{y1_c}(Hz)	0.0101–0.014
$f_{//\_b}$(Hz)	0.011–0.017	f_{y2_c}(Hz)	0.018–0.023
		$f_{//1\_c}$(Hz)	0.0075–0.0105
		$f_{//2\_c}$(Hz)	0.0115–0.0145

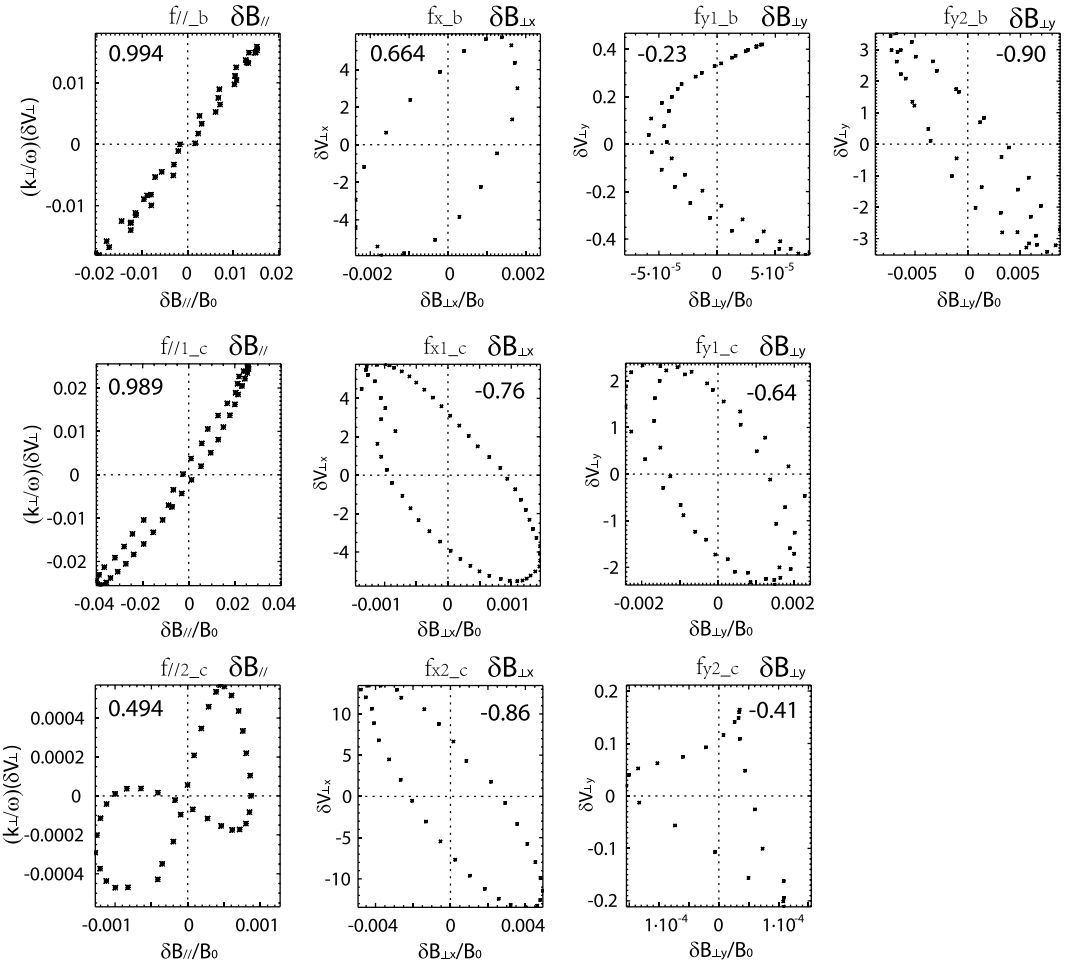

Figure 8. Low-frequency fitting results for (top row) THB and (middle and bottom rows) THC. (left column) Correlations between $(\delta B_{\parallel}/B_0, (k_{\perp}/\omega)\delta V_{\perp})$ for parallel oscillations. (middle column) Scatterplot of $\delta B_{\perp x}/B_0$ versus $\delta V_{\perp x}$ for perpendicular oscillations in *x*. (right column) Scatterplot of $\delta B_{\perp y}/B_0$ versus $\delta V_{\perp y}$ for perpendicular oscillations in *y*.

both spacecraft. The two black rectangles identify the time interval that the low-frequency fitting method was applied. The waveforms of plasma and magnetic pressure are nearly antiphase with slight phase shift. The wave phase velocities obtained from the fitting analysis are ~161 km/s for $f_{//\_b}$ and ~76 km/s for $f_{//1\_c}$, both smaller than the local characteristic velocities. This suggests that slow mode is the dominant mode for the magnetosonic wave observed ahead of the BBF at both spacecraft locations. The similar wave properties observed at different locations indicates that these slow-mode magnetic waves within the Pi2 range are confined within a certain spatial range ahead of the BBF and move earthward together with the BBF. So it is reasonable that these magnetosonic waves are associated with the plasma compression [*Wu and Shay*, 2012] in front of the fast flow. On the other hand, changes can be identified for Alfvenic waves, though those observed at THB was not found at THC location as the BBF became closer to the Earth.

2.3. Pi2 Pulsation Associated With BBFs Moving From Midtail to the Transition Region

Next we examine the waves associated with BBFs when they approach the near-Earth region. We selected an event on 13 March 2009, when a strong auroral expansion onset was observed to the west of the THEMIS spacecraft THC and THD footprints and expanded to the footprints vicinity near ~06:52 UT. Figure 10 shows the observations of a BBF event by these two spacecraft during 20 min interval around onset in the same format as those shown in Figure 6 with THC observations at $X\sim-15.5\ R_E$ on the left and THD at $X\sim-11.5\ R_E$ on the right. Strong bulk flows with peak velocities of nearly 800 km/s are observed by both probes near the same meridian plane. The 60 s time lag for dipolarization allows a fast flow with average velocity of ~530 km/s to propagate ~5 R_E, indicating that the flows observed at the two spacecraft locations are reasonably the same BBF. The magnetic field

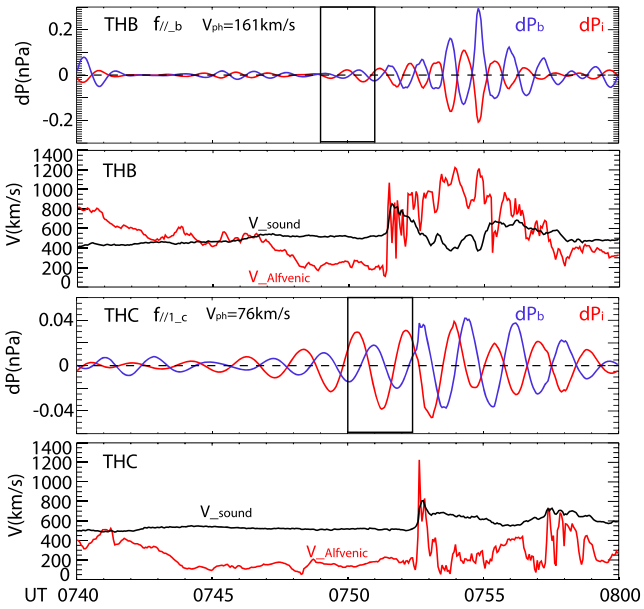

Figure 9. Pressure waveforms filtered in frequency $f_{//}$, Alfvenic, and sound speeds observed by (first and second panels) THB and (third and fourth panels) THC.

spectrograms show wave intensification at discrete frequencies 2–4 min prior to dipolarizations for all the components at both spacecraft locations.

These intensifications are analyzed using low-frequency fitting method in Figure 11. In the previous two events, the parallel magnetic oscillations are the component revealing the property of magnetosonic wave. Thus, we focus on the parallel oscillations in this event. The line plots of wave power obtained from the two spacecraft are stacked in Figure 11 (left column). For each spacecraft, two discrete frequency bands are selected between 0.006 and 0.025 Hz, with $f_{//1\_c}$ = 0.009–0.014 Hz, $f_{//2\_c}$ = 0.017–0.023 Hz, $f_{//1\_d}$ = 0.006–0.01 Hz, and $f_{//2\_d}$ = 0.012–0.018 Hz. The correlation between ($\delta B_{\parallel}/B_0$, $k_{\perp}\delta v_{\perp}/\omega$) for each frequency band in Figure 11 (middle and right columns) all show nearly perfect linear correlation, indicating magnetosonic waves for all the frequency bands. The pressures waveforms and characteristic speeds from both spacecraft in Figure 12 show nearly antiphase dP_i and dP_b for frequency band $f_{//1\_c}$, $f_{//1\_d}$, and $f_{//2\_d}$ during the time interval that the fitting was conducted. The fitted phase velocities are all smaller than the local Alfvenic speed, indicating slow-mode wave. The dP_i and dP_b waveform for $f_{//2\_c}$ frequency band is in phase with fitted phase velocity larger than the local Alfvenic speed and bounded by sound speed, suggesting a fast-mode magnetosonic wave for this frequency band.

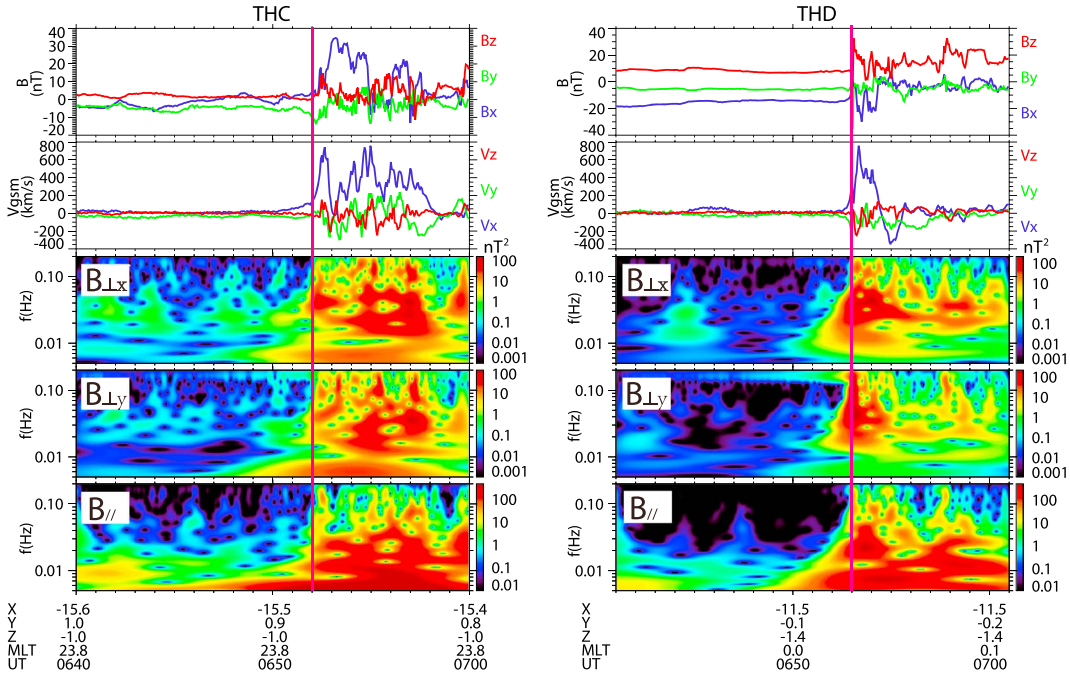

Figure 10. Magnetic field, bulk flow velocity, and three component of magnetic field spectrograms observed by (left) THC and (right) THD on 13 March 2009.

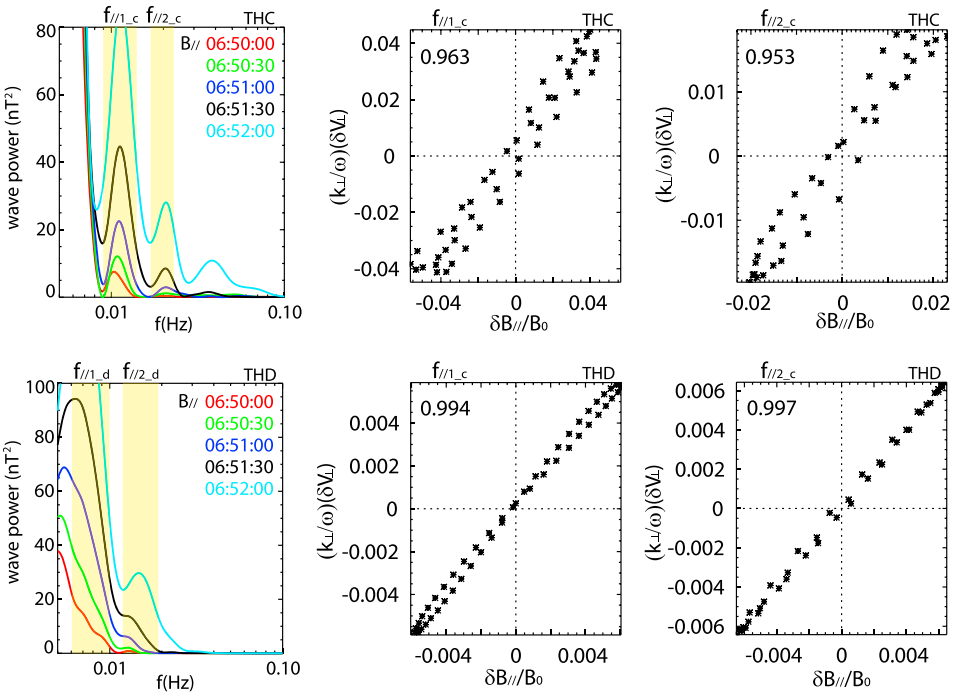

Figure 11. (left column) Line plots of magnetic field parallel component spectrogram sliced at different times from (top row) THC and (bottom row) THD. (middle and right columns) Low-frequency fitting results of correlation between ($\delta B_{\parallel}/B_0$, $(k_{\perp}/\omega)\delta V_{\perp}$) for each selected frequency range with THC in Figure 11 (top row) and THD in Figure 11 (bottom row).

The three events shown above suggest that the low-frequency magnetic oscillations within the Pi2 band are general features associated with earthward moving BBFs that can be observed from midtail near $X\sim-30\,R_E$ to the near-Earth region. The waves are observed 2–4 min before the substantial enhanced flow, and the associated magnetic field dipolarization arrives at the spacecraft location. This suggests that the waves are confined within a localized region ahead of dipolarization and do not propagate very far away. The waves usually initiate within several discrete frequency bands and expand in frequency range as they intensify. As BBFs move earthward, the peaks of the intensified frequency band may vary at different locations possibly due to the ambient plasma environment and BBF velocity changes. For each case, one or more intensified frequency band is found to be magnetosonic waves. Fast mode, slow mode, and coexisting modes are all found for these magnetosonic waves, which we believe result from the plasma compression ahead of the fast flows. Slow mode and a coexisting mode are consistently observed. Pure fast mode only appears at one location for one of the three events.

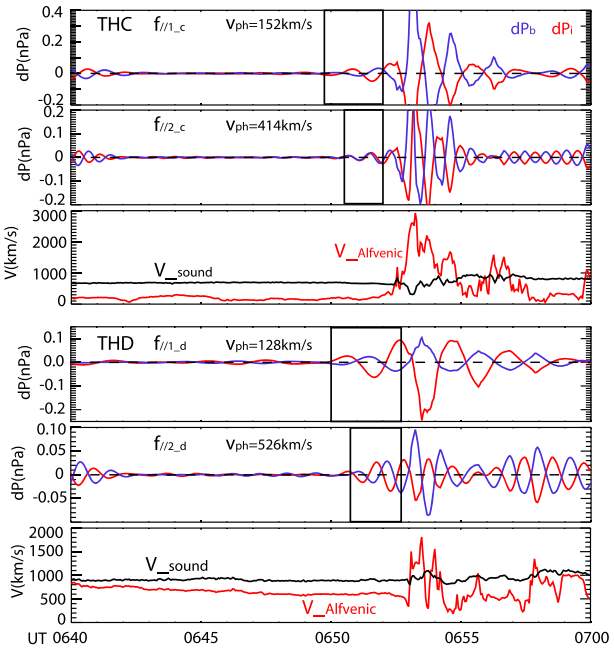

Figure 12. Pressure waveforms filtered at frequencies $f_{//1}$ and $f_{//2}$, Alfvenic, and sound speeds obtained from (first panel–third panels) THC and (fourth–sixth panels) THD.

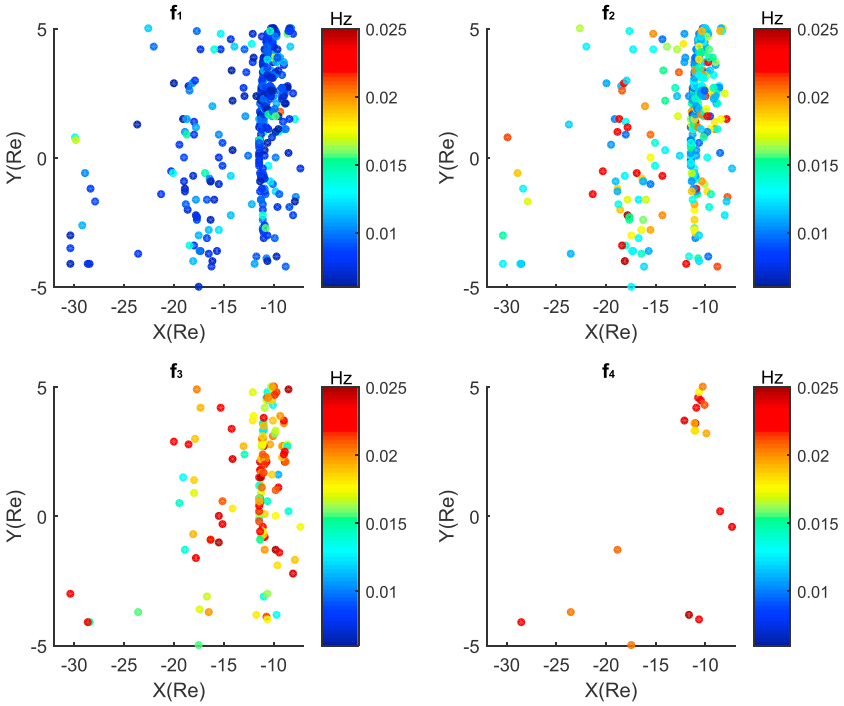

Figure 13. The frequency corresponds to the peak wave power of each discrete pulsations for every event versus the spacecraft locations. f_1 corresponds to the pulsations within the lowest-frequency range for each event. f_2, f_3, and f_4 correspond to oscillations intensified at higher-frequency bands.

3. Statistical Study of Pi2 Pulsations Associated With BBFs in the Entire Plasma Sheet

In order to examine whether the discrete magnetic oscillations within the Pi2 range are common features associated with BBFs in the entire plasma sheet, and what are their basic wave characteristics, we surveyed the data during 2008–2009 THEMIS tail seasons when five spacecraft orbits cover from $X\sim-30\,R_E$ to $X\sim-8\,R_E$ and Y between -5 and $5\,R_E$. 364 BBF events were selected by the criteria that flow peak value larger than 150 km/s with dipolarization more than 5 nT within 10 s, and plasma $\beta > 0.5$. We found that Pi2 pulsations at one or more discrete frequency bands are always observed 1–4 min before a BBF dipolarization front arrives for all the events we have selected. The frequency corresponding to the peak wave power of each discrete pulsations in parallel direction ($\delta B_{//}$) observed from all the events versus the spacecraft locations is shown in Figure 13, where f_1 corresponds to the pulsations at the lowest-frequency band for each event, and f_2, f_3, and f_4 correspond to the pulsations at higher frequencies for the events having more than one intensified frequency bands. The f_1 plot shows that for the majority of events the lowest-frequency oscillations are initiated at a frequency band below 0.01 Hz. Fewer events show discrete oscillations at higher-frequency bands, and only very few cases show the fourth discrete frequency band in the f_4 plot. As for the previous three case studies, we found it common that the intensifications initiated at ~0.01 Hz or higher frequencies are usually stronger than those below 0.01 Hz and may expand toward higher frequencies, which is consistent with *Park et al.*'s [2010] observations. Figure 13 also shows that all the frequencies have no identifiable radial dependence, suggesting that the Pi2 pulsations are commonly associated with BBFs at all radial distances and not simply in the near-Earth transition region.

Figure 14 shows the scatterplot of the correlation coefficient between ($\delta B_{\parallel}/B_0$, $k_{\perp}\delta v_{\perp}/\omega$) for every frequency band shown in Figure 13 versus radial distance $R = \sqrt{X^2 + Y^2}$. The coefficient is calculated during the time interval of $t \geq 1/f_{\min}$ prior to the magnetic dipolarization for each event, where $f_{\min}$ is the minimum frequency of each frequency band. For each of the four frequency groups, the majority of events have the correlation coefficients larger than 0.9, which we define to be the criterion for identifying magnetosonic waves. There is no radial dependence found for the correlation coefficients. The left bar at the bottom right bar plot of each

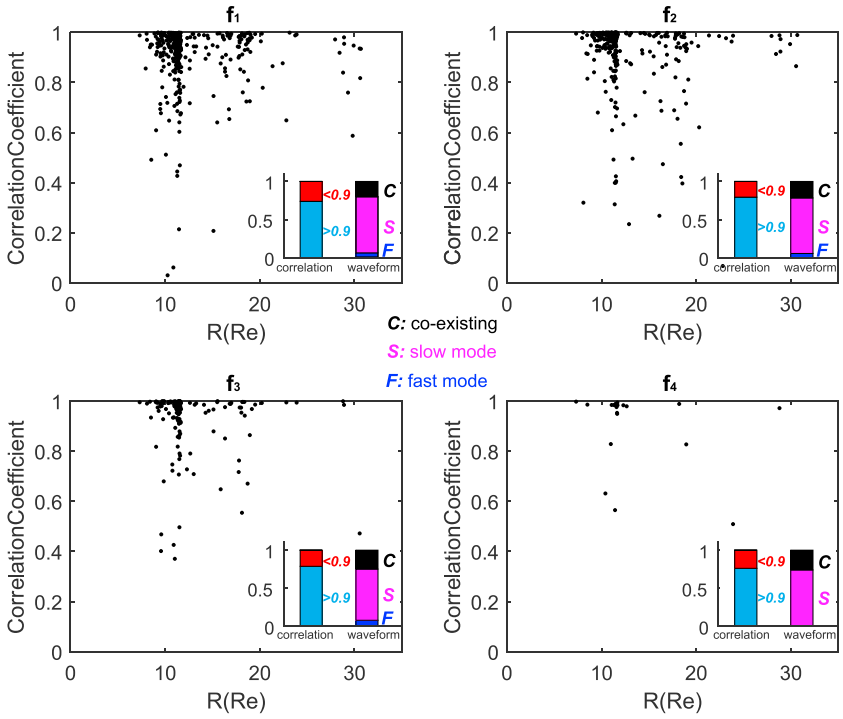

Figure 14. Correlation coefficients obtained from low-frequency fitting for each discrete frequency band shown in Figure 12. The first bar plot in each panel shows the proportion of coefficients larger/smaller than 0.9. The second bar shows the proportion of fast mode, slow mode, and coexisting mode for the identified magnetosonic waves (correlation coefficients >0.9).

panel shows the proportion of the correlation coefficients larger than (light blue) and smaller than (red) 0.9. For every frequency group, over 75% events have correlation coefficient higher than 0.9, indicating that magnetosonic waves are commonly observed associated with BBFs. We further studied the properties of all the magnetosonic waves by examining the phase relation of dP_i and dP_b waveforms. The right bar of each bar plot shows the proportion of different wave properties in each frequency group. *F* in blue denotes fast-mode wave with in-phase dP_i and dP_b; S in magenta denotes slow-mode wave with antiphase dP_i and dP_b; and C in black denotes coexisting mode with dP_i and dP_b neither in phase nor antiphase. In the first three frequency groups, less than 10% of the magnetosonic waves are found to be in fast mode; around 70% are in slow mode; and around 20% are in coexisting mode. In the fourth frequency group, no fast-mode waves are found, the proportions of slow mode and coexisting mode are 74% and 26%. Thus, it can be concluded that slow-mode magnetosonic wave is more likely to be generated ahead of the BBFs.

4. Summary and Discussion

We have examined the low-frequency magnetic oscillations within Pi2 range associated with earthward moving BBFs in the plasma sheet at various radial distances from midtail to the near-Earth region. It was found that Pi2 pulsations usually initiate 1–4 min prior to the dipolarization and the substantial flow enhancement at several discrete frequency bands with lower-frequency oscillations initiating earlier. These waves are always confined within a limited spatial range ahead of BBFs as they move earthward. The MHD wave analysis of the oscillations in each discrete frequency band identifies one or more discrete waves to be magnetosonic waves. Slow mode, fast mode, and coexisting of these two modes are all observed for these waves. The wave properties are quite similar for BBFs observed in both the midtail and near-Earth regions, and no distinguishable wave property changes were found as BBFs move earthward. In our case studies, we have selected BBFs during very quiet time, at substorm onset, and during substorm expansion phase. For various BBFs, their associate Pi2 pulsations show similar characteristics and wave properties under different circumstances, which indicate that the Pi2 pulsations in fact result from the plasma compression due to BBFs instead of substorm onsets.

We further conducted a statistical study of Pi2 pulsations associated with BBFs in the entire plasma sheet within $-30\,R_E < X < -8\,R_E$ and $-5\,R_E < Y < -5\,R_E$. The 364 BBFs with peak earthward bulk velocities larger than 150 km/s and dipolarization over 5 nT were identified near the central plasma sheet ($\beta > 0.5$) regardless of substorm onsets. We found that discrete Pi2 pulsations initiating 1–4 min ahead of the dipolarization and flow burst are common features for BBFs at any locations in the plasma sheet. Among the events we have examined, up to four discrete frequency bands were found for each single BBF. For the majority of our events, the lowest frequency for the discrete pulsation is below 0.01 Hz. The pulsations at around 0.01 Hz or higher frequency have the strongest wave power and expand to a higher-frequency range as time evolves. For all the discrete oscillations, no radial dependence was found regarding frequencies. By applying the MHD low-frequency fitting analysis, we examined the wave properties of each discrete pulsation. We found that over 75% discrete waves are identified as magnetosonic waves, likely due to the plasma compression in front of BBFs. The waveform of thermal and magnetic pressures filtered at each frequency band suggests that over 70% of the magnetosonic waves are in slow mode, less than 10% are in fast mode, and around 20% are coexisting mode. Thus, the slow-mode wave is more likely to be triggered ahead of the BBFs.

These observations strongly suggested that Pi2 pulsations are commonly associated with BBFs in the plasma sheet. As BBFs move earthward, there are always Pi2 pulsations generated ahead of the dipolarization. However, from another aspect, ballooning/interchange instability may not be excluded ahead of earthward moving BBFs while Pi2 pulsations are observed. *Pritchett and Coroniti* [2010] have found using particle-in-cell simulation that the ballooning mode instability can be generated where localized tailward B_z gradient is formed, which is the characteristic feature across the dipolarization front associated with BBFs. Furthermore, their instability mode does not require the conditions of near-Earth plasma sheet with $\beta >$ 50, which are the necessary conditions for the kinetic ballooning mode to occur as suggested by *Cheng and Lui* [1998]. Thus, for the compressional area ahead of BBFs, the instability that is still likely to occur though the kinetic effects is not taken into account. Although this ballooning mode instability proposed by *Pritchett and Coroniti* [2010] is suggested to be associated with lower hybrid drift wave at much higher frequency than Pi2 range, and its relation with the Pi2 pulsations within MHD regime is not clear, these two types of waves could have been both triggered ahead of the BBFs regardless of the locations in the plasma sheet. As for the transition region in the near-Earth plasma sheet, we are not able to distinguish whether the flow enhancements we identified as BBFs in this region are flows penetrating from the more distant tail as suggested by *Runov et al*. [2014] and *Wang et al*. [2015] or flows resulting from the ballooning instability initiated locally in the transition region as suggested by *Saito et al*. [2008]. Regardless of how the fast flows are formed, the Pi2 pulsations associated with the flows in the near-Earth region show wave characteristics very similar to the characteristics seen further out in the tail.

Our results have shown that BBFs are common sources for plasma sheet Pi2 pulsations. However, it is not clear whether these pulsations provide a direct source for the ground Pi2 pulsations. For the majority of BBF events shown above, where slow-mode waves are identified, the plasma sheet Pi2 pulsations do not propagate earthward as the fast-mode waves predicted by *Kepko et al*. [2001] do. For those with Alfven waves present, ground Pi2 pulsations may be triggered at the stations conjugate to the spacecraft locations, but we did not evaluate this possibility.

Acknowledgments

This work at UCLA is supported by NASA grants NNX12AD11G and NNX11AJ12G. We greatly thank THEMIS team for providing all the high-quality data. Data used in this analysis can be obtained from http://themis.ssl.berkeley.edu/index.shtml. We are grateful to Christopher Torrence and Gilbert P. Compo for providing the wavelet analysis software.

Yuming Wang thanks Kazuo Shiokawa and W. Jeffrey Hughes for their assistance in evaluating this paper.

References

Angelopoulos, V. (2008), The THEMIS mission, *Space Sci. Rev.*, *141*(1–4), 5–34, doi:10.1007/s11214-008-9336-1.

Angelopoulos, V., W. Baumjohann, C. F. Kennel, F. V. Coroniti, M. G. Kivelson, R. Pellat, R. J. Walker, H. Lühr, and G. Paschmann (1992), Bursty bulk flows in the inner central plasma sheet, *J. Geophys. Res.*, *97*(A4), 4027–4039, doi:10.1029/91JA02701.

Auster, H. U., et al. (2008), The THEMIS fluxgate magnetometer, *Space Sci. Rev.*, doi:10.1007/s11214-008-9365-9.

Cheng, C. Z., and A. T. Y. Lui (1998), Kinetic ballooning instability for substorm onset and current disruption observed by AMPTE/CCE, *Geophys. Res. Lett.*, *25*, 4091–4094, doi:10.1029/1998GL900093.

Cheng, C. Z., and S. Zaharia (2004), MHD ballooning instability in the plasma sheet, *Geophys. Res. Lett.*, *31*, L06809, doi:10.1029/2003GL018823.

Erickson, G. M., N. C. Maynard, W. J. Burke, G. R. Wilson, and M. A. Heinemann (2000), Electromagnetics of substorm onsets in the near-geosynchronous plasma sheet, *J. Geophys. Res.*, *105*(A11), 25,265–25,290, doi:10.1029/1999JA000424.

Holter, Ø., C. Altman, A. Roux, S. Perraut, A. Pedersen, H. Pécseli, B. Lybekk, J. Trulsen, A. Korth, and G. Kremser (1995), Characterization of low frequency oscillations at substorm breakup, *J. Geophys. Res.*, *100*(A10), 19,109–19,119, doi:10.1029/95JA00990.

Kepko, L., and M. Kivelson (1999), Generation of Pi2 pulsations by bursty bulk flows, *J. Geophys. Res.*, *104*(A11), 25,021–25,034, doi:10.1029/1999JA900361.

Kepko, L., M. G. Kivelson, and K. Yumoto (2001), Flow bursts, braking, and Pi2 pulsations, *J. Geophys. Res.*, *106*(A2), 1903–1915, doi:10.1029/2000JA000158.

Kim, K.-H., K. Takahashi, D.-H. Lee, P. R. Sutcliffe, and K. Yumoto (2005), Pi2 pulsations associated with poleward boundary intensifications during the absence of substorms, *J. Geophys. Res.*, *110*, A01217, doi:10.1029/2004JA010780.

Lee, K.-W., and L.-N. Hau (2008), Characteristics of magnetohydrodynamic waves in Harris-type current sheet with guide magnetic field *By*, *J. Geophys. Res.*, *113*, A12209, doi:10.1029/2008JA013459.

Liang, J., W. W. Liu, E. F. Donovan, and E. Spanswick (2009), In-situ observation of ULF wave activities associated with substorm expansion phase onset and current disruption, *Ann. Geophys.*, *27*, 2191–2204.

Lui, A. T. Y., and A.-H. Najmi (1997), Time-frequency decomposition of signals in a current disruption event, *Geophys. Res. Lett.*, *24*(24), 3157–3160, doi:10.1029/97GL03229.

Lyons, L. R., Nishimura, Y., Xing, X., Shi, Y., Gkioulidou, M., Wang, C.-P., Kim, H.-J., Zou, S., Angelopoulos, V., and Donovan, E. (2012) Auroral disturbances as a manifestation of interplay between large-scale and mesoscale structure of magnetosphere-ionosphere electrodynamical coupling, in *Auroral Phenomenology and Magnetospheric Processes: Earth And Other Planets*, edited by A. Keiling et al., AGU, Washington, D. C., doi:10.1029/2011GM001152

McFadden, J. P., et al. (2008), The THEMIS ESA plasma instrument and in-flight 244 calibration, *Space Sci. Rev.*, doi:10.1107/s11214-008-9440-2.

Nishimura, Y., L. R. Lyons, T. Kikuchi, V. Angelopoulos, E. Donovan, S. Mende, P. J. Chi, and T. Nagatsuma (2012), Formation of substorm Pi2: A coherent response to auroral streamers and currents, *J. Geophys. Res.*, *117*, A09218, doi:10.1029/2012JA017889.

Nishimura, Y., et al. (2014), Coordinated ionospheric observations indicating coupling between preonset flow bursts and waves that lead to substorm onset, *J. Geophys. Res. Space Physics*, *119*, 3333–3344, doi:10.1002/2014JA019773.

Panov, E. V., V. A. Sergeev, P. L. Pritchett, F. V. Coroniti, R. Nakamura, W. Baumjohann, V. Angelopoulos, H. U. Auster, and J. P. McFadden (2012), Observations of kinetic ballooning/interchange instability signatures in the magnetotail, *Geophys. Res. Lett.*, *39*, L08110, doi:10.1029/2012GL051668.

Panov, E. V., A. V. Artemyev, W. Baumjohann, R. Nakamura, and V. Angelopoulos (2013), Transient electron precipitation during oscillatory BBF braking: THEMIS observations and theoretical estimates, *J. Geophys. Res. Space Physics*, *118*, 3065–3076, doi:10.1002/jgra.50203.

Panov, E. V., W. Baumjohann, M. V. Kubyshkina, R. Nakamura, V. A. Sergeev, V. Angelopoulos, K.-H. Glassmeier, and A. A. Petrukovich (2014), On the increasing oscillation period of flows at the tailward retreating flux pileup region during dipolarization, *J. Geophys. Res. Space Physics*, *119*, 6603–6611, doi:10.1002/2014JA020322.

Park, M. Y., D.-Y. Lee, S. Ohtani, and K. C. Kim (2010), Statistical characteristics and significance of low-frequency instability associated with magnetic dipolarizations in the near-Earth plasma sheet, *J. Geophys. Res.*, *115*, A11203, doi:10.1029/2010JA015566.

Pritchett, P. L., and F. V. Coroniti (2010), A kinetic ballooning/interchange instability in the magnetotail, *J. Geophys. Res.*, *115*, A06301, doi:10.1029/2009JA014752.

Runov, A., V. Angelopoulos, M. I. Sitnov, V. A. Sergeev, J. Bonnell, J. P. McFadden, D. Larson, K.-H. Glassmeier, and U. Auster (2009), THEMIS observations of an earthward propagating dipolarization front, *Geophys. Res. Lett.*, *36*, L14106, doi:10.1029/2009GL038980.

Runov, A., V. A. Sergeev, V. Angelopoulos, K.-H. Glassmeier, and H. J. Singer (2014), Diamagnetic oscillations ahead of stopped dipolarization fronts, *J. Geophys. Res. Space Physics*, *119*, 1643–1657, doi:10.1002/2013JA019384.

Saito, M. H., Y. Miyashita, M. Fujimoto, I. Shinohara, Y. Saito, and T. Mukai (2008), Modes and characteristics of low-frequency MHD waves in the near-Earth magnetotail prior to dipolarization: Fitting method, *J. Geophys. Res.*, *113*, A06201, doi:10.1029/2007JA012778.

Saito, T., T. Sakurai, and Y. Koyama (1976), Mechanism of association between Pi2 pulsation and magnetospheric substorm, *J. Atmos. Sol. Terr. Phys.*, *38*, 1265–1277.

Seboldt, W. (1990), Nonlocal analysis of low-frequency waves in the plasma sheet, *J. Geophys. Res.*, *95*(A7), 10,471–10,479, doi:10.1029/JA095iA07p10471.

Shiokawa, K., I. Shinohara, T. Mukai, H. Hayakawa, and C. Z. Cheng (2005), Magnetic field fluctuations during substorm-associated dipolarizations in the nightside plasma sheet around $X = -10\ R_E$, *J. Geophys. Res.*, *110*, A05212, doi:10.1029/2004JA010378.

Sigsbee, K., C. A. Cattell, D. Fairfield, K. Tsuruda, and S. Kokubun (2002), Geotail observations of low-frequency waves and high-speed earthward flows during substorm onsets in the near magnetotail from 10 to 13 R_E, *J. Geophys. Res.*, *107*(A7), 1141, doi:10.1029/2001JA000166.

Sutcliffe, P. R., and L. R. Lyons (2002), Association between quiet-time Pi2 pulsations, poleward boundary intensifications, and plasma sheet particle fluxes, *Geophys. Res. Lett.*, *29*(9), 1293, doi:10.1029/2001GL014430.

Torrence, C., and G. Compo (1998), A practical guide to wavelet analysis, *Bull. Am. Meteorol. Soc.*, *79*, 61–78.

Uritsky, V. M., J. Liang, E. Donovan, E. Spanswick, D. Knudsen, W. Liu, J. Bonnell, and K. H. Glassmeier (2009), Longitudinally propagating arc wave in the pre-onset optical aurora, *Geophys. Res. Lett.*, *36*, L21103, doi:10.1029/2009GL040777.

Wang, G. Q., Y. S. Ge, T. L. Zhang, R. Nakamura, M. Volwerk, W. Baumjohann, A. M. Du, and Q. M. Lu (2015), A statistical analysis of Pi2-band waves in the plasma sheet and their relation to magnetospheric drivers, *J. Geophys. Res. Space Physics*, *120*, doi:10.1002/2014JA020753.

Wolf, R. A., C. X. Chen, and F. R. Toffoletto (2012), Thin filament simulations for Earth's plasma sheet: Interchange oscillations, *J. Geophys. Res.*, *117*, A02215, doi:10.1029/2011JA016971.

Wu, P., and M. A. Shay (2012), Magnetotail dipolarization front and associated ion reflection: Particle-in-cell simulations, *Geophys. Res. Lett.*, *39*, L08107, doi:10.1029/2012GL051486.

Xing, X., J. Liang, E. Spanswick, L. Lyons, and V. Angelopoulos (2013), Auroral wave structures and ballooning instabilities in the plasma sheet, *J. Geophys. Res. Space Physics*, *118*, 6319–6326, doi:10.1002/2013JA019068.

Yoeman, T. K., M. P. Freeman, G. D. Reeves, M. Lester, and D. Orr (1994), A comparison of midlatitude Pi2 pulsations and geostationary orbit particle injections as substorm indicators, *J. Geophys. Res.*, *99*, 4085–4093, doi:10.1029/93JA03233.

Zesta, E., E. Donovan, L. Lyons, G. Enno, J. S. Murphree, and L. Cogger (2002), Two-dimensional structure of auroral poleward boundary intensifications, *J. Geophys. Res.*, *107*(A11), 1350, doi:10.1029/2001JA000260.